JOURNAL OF GUIDANCE, CONTROL, AND DYNAMICS
Vol. 36, No. 3, May–June 2013

Analysis of Energy-Optimal Aircraft Landing Operation Trajectories

Yiming Zhao* and Panagiotis Tsiotras†
Georgia Institute of Technology, Atlanta, Georgia 30332-0150

DOI: 10.2514/1.57779

This paper presents a method for the energy-optimal operation of a fixed-wing aircraft tracking a prescribed landing path in the three-dimensional space with a fixed time of arrival. The problem is converted to an optimal control problem with one state variable, which is subject to state and control input constraints along the path. It is shown that the solution to this energy-optimal tracking problem provides a good approximation to the minimum-fuel problem. The switching structure of the optimal solution is analyzed, and a semi-analytical method is proposed for computing the optimal solution. Compared to standard numerical optimization methods the proposed method is guaranteed to converge to the optimal solution, and it is computationally much more efficient. Numerical examples are presented to demonstrate the validity of the proposed approach. As verified by these numerical results the proposed energy-optimal solution can help improve aircraft fuel efficiency during the landing phase.

Nomenclature

C_D	=	drag coefficient
C_{D_0}	=	zero lift drag coefficient
C_L	=	lift coefficient
$C_{L_{\max}}$	=	maximum lift coefficient
$C_{L_{\min}}$	=	minimum lift coefficient
C_L^*	=	optimal lift coefficient
D	=	specific drag force, N/kg
$\tilde{D}$	=	specific drag force along singular arc, N/kg
E	=	kinetic energy per unit mass, J/kg
E^*	=	optimal specific kinetic energy, J/kg
E_L^*	=	maximum-time specific kinetic energy, J/kg
$E_{L_r}^*$	=	maximum-time specific kinetic energy of the relaxed problem, J/kg
E_r^*	=	energy-optimal solution of the relaxed problem, J/kg
E_U^*	=	minimum-time specific kinetic energy, J/kg
$E_{U_r}^*$	=	minimum-time specific kinetic energy of the relaxed problem, J/kg
$\tilde{E}$	=	singular specific kinetic energy arc, J/kg
g	=	gravity acceleration, m/s^2
$\underline{g}_{\Gamma_L}$	=	kinetic energy lower bound relaxed on the set Γ_L, J/kg
$\bar{g}_{\Gamma_U}$	=	kinetic energy upper bound relaxed on the set Γ_U, J/kg
$\underline{g}_w$	=	lower bound of kinetic energy, J/kg
$\bar{g}_w$	=	upper bound of kinetic energy, J/kg
K	=	induced drag coefficient
M_a	=	Mach number
m	=	mass, kg
S	=	wing surface area, m^2
s	=	path coordinate, m
s_f	=	path length, m
T	=	thrust, N
$T_{\max}$	=	maximum thrust, N
$T_{\min}$	=	minimum thrust, N
T_w	=	thrust for maximum speed travel, N
$\underline{T}_w$	=	thrust for minimum speed travel, N
T^*	=	optimal thrust, N
$\tilde{T}$	=	singular thrust control, N
t	=	time, s
t_f	=	final time, s
x, y, z	=	position, m
γ	=	path angle, rad
λ_E	=	costate variable associated with E
λ_t	=	costate variable associated with t
$\lambda_{t_r}^*$	=	optimal t-costate of the relaxed problem
v	=	speed, m/s
ρ	=	air density, kg/m^3
ϕ	=	bank angle, rad
$\phi_{\max}$	=	maximum bank angle, rad
$\phi_{\min}$	=	minimum bank angle, rad
ϕ^*	=	optimal bank angle, rad
ψ	=	heading angle, rad

I. Introduction

WITH rising fuel costs it is desirable to improve the fuel efficiency of current aircraft operations subject to aircraft performance and scheduling constraints. Such a problem can be naturally cast as an optimal motion planning problem, which is a common problem encountered in many industrial and transportation systems, including robotic arms [1–4], ground vehicles [5–8], and aircraft [9,10]. Although optimal motion planning problems can be solved directly using numerical optimization techniques [11–17] the number of the required computations may grow to impractical levels, especially for real-time applications. Hence, a hybrid approach is commonly adopted in practice, according to which the motion planning task is decomposed into multiple levels [18,19]. At the higher level only the geometric aspects of the path are considered, whereas the lower (path-tracking) level deals with the system dynamics and the state and control constraints, and it generates the time parameterization of the path provided by the higher (geometric) level planner. This paper focuses on the aircraft path-tracking problem at the lower level. Therefore, throughout the paper, it is assumed that the path to be followed is given by the geometric level path planner. The assumption that the path is given (and its calculation is not part of the optimization process) and is not as unusual or atypical as one may initially think. Commercial airliners during the terminal landing phase are required to follow strict air traffic control (ATC) rules, which guide the airplanes with "virtual" three-dimensional corridors all the way to the landing strip. Furthermore, because our approach leads to very fast computation of feasible trajectories, one can use the approach over new, locally modified paths repeatedly until a satisfactory path is found. Zhao and

Received 30 January 2012; revision received 20 June 2012; accepted for publication 9 July 2012; published online 28 February 2013.

*Ph.D. Student, School of Aerospace Engineering; currently Adjunct Member Research Staff, Mitsubishi Electric Research Laboratories, Cambridge, MA; yzhao7@gatech.edu.

†Dean's Professor, School of Aerospace Engineering; tsiotras@gatech.edu. Fellow AIAA.

Tsiotras [20] discuss a computationally efficient approach to modify the original path such that certain constraints are met. Finally, if necessary, the computed trajectories by the proposed approach can be used as an initial guess for a higher fidelity optimal trajectory generation solver [21]. Hence, from now on it will be assumed that the path is given. Note, however, that this does not mean that the *trajectory* to be followed is given. A trajectory requires a time-parameterized path, and it is, indeed, the main goal of this paper to provide such a time parameterization so as to meet certain optimality specifications.

Given a path the minimum-time path-tracking problem for robotic manipulators, ground vehicles, and aircraft has been studied in [1–3,8,22]. The optimal solution to these problems can help improve plant productivity [1–3], racing car performance [8], or achieve faster aircraft landing in case of an emergency [22]. These solutions maximize, pointwise, the speed along the path and do not contain any singular arcs. When tracking time is not of primary concern it is often desirable to minimize the energy or the fuel consumption of the system. Along this direction the minimum-work operation problem has been studied in [5–7]. Unlike the solution to the minimum-time problem, minimum-work, or minimum-energy solutions usually contain singular control arcs, in addition to the bang–bang control arcs. As it is typically the case for problems with singular arcs, it is difficult to determine the optimal sequence in which these singular arcs appear, in combination with the bang–bang arcs, in the optimal solution and the corresponding optimal switching times. Numerical techniques are usually required for solving optimal control problems involving both bang–bang and singular arcs. When the travel time is free the explicit expression of a singular arc can be solved analytically. In the case of fixed travel time, which is most important for scheduled or terminal ATC operations, the singular arc(s) cannot be computed directly, and a numerical procedure must be used to compute the singular arc(s) such that the desired travel time and boundary conditions are satisfied.

When using numerical methods to solve optimal singular control problems, initially, a control switching structure is guessed based on the analytic expression of the singular control. Subsequently, the guessed switching structure is applied to solve the singular control problem [23]. These numerical methods are time consuming and require extensive knowledge and experience from the part of the user to obtain the actual optimal solution. On the other hand, an analytical optimal control approach [5–7], although less general than purely numerical methods, can provide more accurate information about the singular arcs and switching times in the optimal solution, and, thus, it is more reliable and efficient.

This paper considers the problem of minimum-energy path-tracking for fixed-wing aircraft with fixed time of arrival (TOA). As in [22], a scalar functional optimization problem is formulated and solved semi-analytically using optimal control theory. Because fuel consumption is closely related to the engine's mechanical work counteracting the effects of air drag the issue of fuel efficiency can also be addressed (at least approximately) by solving this minimum-energy problem. Compared to the somewhat similar minimum-work problem for train operations [5–7] in which the initial and final speed are both zero and only the upper speed limit can be active in the middle of the optimal solution, in the aircraft path-tracking problem considered in this paper both the initial and final values of the speed are nonzero, and both upper and lower nonzero speed bounds exist and can be active along the path. Hence, the aircraft minimum-energy solution exhibits a more complicated switching structure than the one illustrated in [5–7].

The main contributions of this paper include: 1) a new result regarding the admissible switching structure in the optimal solution of the minimum-energy aircraft path-tracking problem with fixed TOA, 2) a partial relaxation technique for identifying the subintervals on which the speed constraint is active, 3) the characterization of the relation between optimal solutions of minimum-time, maximum-time, and minimum-energy path-tracking problems, and finally, 4) the development of an efficient and reliable algorithm for computing the overall minimum-energy solution. The current paper should be viewed as a companion paper to [24] (see also [22]), where some of the basic results used in this paper were first derived. To avoid unnecessary repetition the reader will often be referred to [24] for some of the missing details.

The rest of this paper is organized as follows: the aircraft dynamics is introduced in Sec. II. The aircraft minimum-energy fixed TOA path-tracking problem is formulated as an optimal control problem in Sec. III. In Sec. IV, the optimal solution of the minimum-energy problem is characterized. The optimal switching structure is also determined for the case when the state constraints are not active. The solution of the complete problem, that is, when constrained arcs are part of the optimal solution, is given in Sec. VI. The answer hinges on the solution of a relaxed problem, which is formulated in Sec. V. Based on the results of Sec. VI a minimum-energy path-tracking algorithm is proposed in Sec. VII. Finally, the validity of the proposed methodology is tested using numerical experiments, and the results are presented at the end of the paper.

II. Aircraft Dynamics

A point-mass model of a fixed-wing aircraft is given by the following equations of motion [25]:

$$\dot{x} = v\cos\gamma\cos\psi \tag{1}$$

$$\dot{y} = v\cos\gamma\sin\psi \tag{2}$$

$$\dot{z} = v\sin\gamma \tag{3}$$

$$\dot{v} = \frac{1}{m}[T - F_D(C_L, v, z) - mg\sin\gamma] \tag{4}$$

$$\dot{\gamma} = \frac{1}{mv}[F_L(C_L, v, z)\cos\phi - mg\cos\gamma] \tag{5}$$

$$\dot{\psi} = -\frac{F_L(C_L, v, z)\sin\phi}{mv\cos\gamma} \tag{6}$$

where x and y denote the position of the aircraft in the horizontal plane, z is the altitude, v is the aircraft speed, γ is the flight path angle, ψ is the heading angle, and ϕ is the aircraft bank angle. In the previous simplified model the effect of the wind is not included.

The aerodynamic lift force $F_L(C_L, v, z)$ and the drag force $F_D(C_L, v, z)$ are given by

$$F_L(C_L, v, z) = \frac{1}{2}\rho(z)v^2SC_L \tag{7}$$

$$F_D(C_L, v, z) = \frac{1}{2}\rho(z)v^2SC_D = \frac{1}{2}\rho(z)v^2S(C_{D_0} + KC_L^2) \tag{8}$$

where $\rho(z)$ is the air density given as a function of z, C_{D_0} and K are parameters describing the aerodynamic properties of the aircraft, and S is the main wing surface area. The drag coefficients C_{D_0} and K depend continuously on the Mach number and, hence, are continuous functions of the airspeed and the path length s. The control inputs in this model are the lift coefficient C_L, the bank angle ϕ, and the thrust T. It is required that the aircraft speed satisfies the bounds $v(s) \in [v_{\min}(z), v_{\max}(z)]$, where $v_{\min}(z)$ and $v_{\max}(z)$ are altitude-dependent minimum and maximum speeds, respectively, and

$$C_L \in [C_{L_{\min}}, C_{L_{\max}}], \qquad \phi \in [\phi_{\min}, \phi_{\max}], \qquad T \in [T_{\min}, T_{\max}] \tag{9}$$

where $C_{L_{\min}}$, $C_{L_{\max}}$, $\phi_{\min}$, $\phi_{\max}$, $T_{\min}$, and $T_{\max}$ are (possibly path-dependent) bounds on the associated control inputs. It is assumed that $C_{L_{\min}} \le 0 \le C_{L_{\max}}$, $-\pi/2 < \phi_{\min} < 0 < \phi_{\max} < \pi/2$, $0 \le T_{\min} < T_{\max}$, and $\gamma \in (-\pi/2, \pi/2)$. These conditions are generic for a civil fixed-wing aircraft in normal/maneuverable flight.

Let now $(x(s), y(s), z(s))$ denote a three-dimensional geometric path, which is parameterized by its natural path length coordinate $s \in [s_0, s_f] \subset \mathbb{R}_+$. The main objective of this paper is to find a time parameterization of the path, or equivalently, a function $s(t)$ with $s(0) = s_0$ and $s(t_f) = s_f$, where $t \in [0, t_f]$, and t_f is the desired TOA such that the corresponding time-parameterized trajectory $(x(s(t)), y(s(t)), z(s(t)))$ minimizes the total energy or mechanical work, while flying along the path and without violating any state or control constraints. The path coordinate s is related to the speed v as follows

$$s(t) = \int_{t_0}^{t} v(\tau)\,\mathrm{d}\tau$$

The key step for solving this problem is the optimization of the speed profile $v(s)$ along the path. Because the given path is naturally parameterized using the path coordinate s instead of time the equations of motion can be rewritten with respect to s as follows (where prime denotes differentiation with respect to s [24]):

$$x' = \cos\gamma\,\cos\psi \tag{10}$$

$$y' = \cos\gamma\,\sin\psi \tag{11}$$

$$z' = \sin\gamma \tag{12}$$

$$v' = \frac{1}{mv}[T - F_D(C_L, v, \rho) - mg\,\sin\gamma] \tag{13}$$

$$\gamma' = \frac{1}{mv^2}[F_L(C_L, v, \rho)\cos\phi - mg\,\cos\gamma] \tag{14}$$

$$\psi' = -\frac{F_L(C_L, v, \rho)\sin\phi}{mv^2\,\cos\gamma} \tag{15}$$

For convenience of notation let $E \triangleq v^2/2$ denote the specific kinetic energy per unit mass of the aircraft. It has been shown in [22] that the lift coefficient, bank angle, and speed constraints can be reduced to lower and upper bounds on the specific kinetic energy E as follows:

$$E(s) - \bar{g}_w(s) \le 0 \tag{16}$$

$$\underline{g}_w(s) - E(s) \le 0 \tag{17}$$

for all $s \in [s_0, s_f]$, where $\bar{g}_w(s)$ and $\underline{g}_w(s)$ are path-dependent bounds on the specific kinetic energy, which are determined from the path geometry, and the constraints on the speed, bank angle, and lift coefficient. The derivative of E satisfies the following ordinary differential equation [22]:

$$E'(s) = \frac{T(s)}{m} - D(E(s), s) - g\,\sin\gamma \tag{18}$$

where the prime denotes the derivative with respect to s, and

$$D(E, s) = c_1(E(s), s)E(s) + \frac{c_2(E(s), s)}{E(s)} + c_3(E(s), s) \tag{19}$$

with

$$c_1(E, s) \triangleq \frac{C_{D_0}(E, s)\rho(s)S}{m} + \frac{4K(E, s)m}{\rho(s)S}(\gamma'^2(s) + \cos^2\gamma(s)\psi'^2(s)) \tag{20}$$

$$c_2(E, s) \triangleq \frac{K(E, s)mg^2\cos^2\gamma(s)}{\rho(s)S} \tag{21}$$

$$c_3(E, s) \triangleq \frac{4K(E, s)m\gamma'(s)g\,\cos\gamma(s)}{\rho(s)S} \tag{22}$$

It will be assumed that the path is chosen such that $D(E, s)$ and $\partial D/\partial E$ are continuous with respect to s. Once the optimal specific kinetic energy $E^*(s)$ is obtained the optimal thrust profile $T^*(s)$ along the path can be determined using Eq. (18). Subsequently, the other optimal control inputs can also be computed using inverse dynamics as follows [21,22]:

$$\phi^*(s) = -\arctan\left(\frac{\cos\gamma(s)\psi'(s)}{\gamma'(s) + g\,\cos\gamma(s)/v^{*2}(s)}\right) \tag{23}$$

$$C_L^*(s) = \frac{2m}{\rho(s)S\,\cos\phi^*(s)}\left(\gamma'(s) + \frac{g\,\cos\gamma(s)}{v^{*2}(s)}\right) \tag{24}$$

The following proposition, taken from [22], is important for characterizing the minimum-time optimal solution, which is used to construct the minimum-energy optimal solution later in this paper.

Proposition II.1: Consider the minimum-time path-tracking problem along a given path $(x(s), y(s), z(s))$, where $(x(s_0), y(s_0), z(s_0))$ and $(x(s_f), y(s_f), z(s_f))$ are given. Let T^* be the optimal control, and let $(s_a, s_b] \subseteq [s_0, s_f]$. If neither the upper nor the lower speed limit constraint is active for any $s \in (s_a, s_b]$ then T^* is bang–bang and contains at most one switch, which is from $T_{\max}$ to $T_{\min}$.

III. Problem Formulation

In this section, the energy-optimal aircraft path-tracking problem with fixed TOA is formulated as an optimal control problem, which provides an approximate solution to the minimum-fuel problem. Most modern civil airliners are powered by high-bypass turbofan engines for better fuel economy. The fuel consumption rate for this type of engine is given by [26]

$$\dot{f} = -\eta T \tag{25}$$

where f is the fuel weight, η is the *installed thrust specific fuel consumption*, which varies with airspeed, altitude, type of engine, and throttle conditions, and it is given by

$$\eta = (a + bM_a)\sqrt{\eta_0/(1 + cM_a^2)} \tag{26}$$

where M_a is the Mach number and a, b, c are constants depending on the engine type. In Eq. (26), $\eta_0 = \eta_0(z, M_a)$ varies with altitude and Mach number and can be determined from lookup data tables [26]. The fuel consumption models for other types of jet engines are similar to Eqs. (25) and (26) but with different parameters.

With the above model the fuel consumption during the landing phase can be estimated by

$$J_f = \int_{t_0}^{t_f} -\dot{f}(t)\,\mathrm{d}t = \int_{t_0}^{t_f} \eta(t)T(t)\,\mathrm{d}t \tag{27}$$

From Eq. (27) it is clear that the minimum-fuel problem is equivalent to the minimization of the weighted thrust history, where the weight $\eta(t)$ is given in Eq. (26). The solution to this problem requires the use of purely numerical techniques. To avoid this difficulty this paper seeks to minimize, instead, the total energy (mechanical work) required to fly along the path, which is given by

$$J_w = \int_{t_0}^{t_f} v(t)T(t)\,\mathrm{d}t = \int_{s_0}^{s_f} T(s)\,\mathrm{d}s \tag{28}$$

As demonstrated in [27] the optimal speed profile of the minimum-fuel optimization problem contains singular arcs on which most of the fuel savings is achieved. It was observed in our numerical studies that the airspeed changes slowly along these singular arcs, in which case the singular arcs of the fuel-optimal problem can be approximated by those of the energy-optimal problem. As a result, the minimization of the energy cost function (28) is expected to provide a reasonably good approximation to the fuel optimization problem (27). This is verified by the numerical results in Sec. VIII. Henceforth, this paper focuses on minimizing Eq. (28).

During the landing process the change of mass due to fuel consumption is usually negligible when compared to the total mass of the aircraft. Hence, the effect of mass change on the specific kinetic energy dynamics in Eq. (18) can be neglected, and it is assumed that m is constant during the landing phase. The validity of such an assumption is justified in [27], which reported that the mass change has little influence on the fuel-optimal trajectory during the climb and descent phases. It needs to be noted, however, that this assumption would be invalid during the long cruise phase [28].

To account for the fixed final time the flight time t is treated as a state variable in an augmented system with the additional differential equation

$$t'(s) = \frac{1}{\sqrt{2E(s)}}$$

With the above assumptions the minimum-energy aircraft path-tracking problem with fixed TOA can be formulated as an optimal control problem involving two differential equations, two algebraic constraints, four boundary conditions, and two control constraints, as follows.

Problem 1 (Minimum energy path-tracking problem with fixed TOA) Consider the following optimal control problem in Lagrange form:

$$\min_T \int_{s_0}^{s_f} T(s)\,\mathrm{d}s \tag{29}$$

$$\text{subject to } E'(s) = \frac{T(s)}{m} - D(E(s), s) - g\,\sin\gamma(s) \tag{30}$$

$$t'(s) = \frac{1}{\sqrt{2E(s)}} \tag{31}$$

$$E(s) - \bar{g}_w(s) \le 0 \tag{32}$$

$$\underline{g}_w(s) - E(s) \le 0 \tag{33}$$

$$E(s_0) = v_0^2/2 \tag{34}$$

$$E(s_f) = v_f^2/2 \tag{35}$$

$$T_{\min}(s) \le T(s) \le T_{\max}(s) \tag{36}$$

$$t(s_0) = 0 \tag{37}$$

$$t(s_f) = t_f \tag{38}$$

Throughout this work it is assumed that the optimal solution to Problem 1 exists. In the rest of this paper, it will be shown that there exists a unique feasible solution, which satisfies all optimality conditions and constraints, hence this solution must be optimal.

IV. Optimality Conditions

This section focuses on the simple case of Problem 1 when the state constraints are not active. For this case, the optimal control, as well as the switching structure, is derived based on the optimality conditions. Because the optimal control may contain singular arcs the generalized Legendre–Clebsch condition [29,30] is also checked to verify the optimality of the singular arcs.

A. Optimal Control Formulation

Consider first the case when the state constraints (32) and (33) are inactive. The Hamiltonian for Problem 1 is given by

$$\begin{aligned} H(E,t,\lambda_E,\lambda_t,T,s) &= T + \lambda_E\left(\frac{T}{m} - D(E,s) - g\,\sin\gamma(s)\right) + \frac{\lambda_t}{\sqrt{2E}} \\ &= \left(1+\frac{\lambda_E}{m}\right)T - \lambda_E(D(E,s) + g\,\sin\gamma(s)) + \frac{\lambda_t}{\sqrt{2E}} \end{aligned}$$

where λ_E and λ_t are the costates corresponding to the dynamics for E and t, respectively. The costate dynamics are given by

$$\lambda_E' = -\frac{\partial H}{\partial E} = \lambda_E\frac{\partial D}{\partial E} + \frac{1}{2\sqrt{2}}E^{-3/2}\lambda_t \tag{39}$$

$$\lambda_t' = -\frac{\partial H}{\partial t} = 0 \tag{40}$$

Therefore, the costate λ_t is constant. The switching function is given by

$$\frac{\partial H}{\partial T} = 1 + \frac{\lambda_E}{m} \tag{41}$$

By Pontryagin's maximum principal (PMP) the extremal control is given by

$$T = \begin{cases} T_{\max}, & 1+\lambda_E/m < 0, \\ \tilde{T}, & 1+\lambda_E/m = 0, \\ T_{\min}, & 1+\lambda_E/m > 0 \end{cases} \tag{42}$$

where $\tilde{T}$ is the singular control.

Suppose that the optimal specific kinetic energy E^* contains a singular arc represented by $\tilde{E}$, for example, $E^*(s) = \tilde{E}(s)$ on some subinterval of $[s_0, s_f]$. For notational convenience, let us denote

$$\frac{\partial^k \tilde{D}}{\partial E^k} = \left.\frac{\partial^k D}{\partial E^k}\right|_{(\tilde{E}(s),s)}, \qquad k = 1, 2$$

and let λ_t^* be the optimal costate value, then the switching function (41) is identically zero along the singular arc. Hence, the derivative of the switching function must also vanish on singular arcs, which yields

$$\begin{aligned} \frac{\mathrm{d}}{\mathrm{d}s}\left(\frac{\partial H}{\partial T}\right) &= \frac{1}{m}\left(\lambda_E\frac{\partial \tilde{D}}{\partial E} + \frac{1}{2\sqrt{2}}\tilde{E}^{-3/2}\lambda_t\right) \\ &= -\frac{\partial \tilde{D}}{\partial E} + \frac{1}{2\sqrt{2m}}\tilde{E}^{-3/2}\lambda_t \equiv 0 \end{aligned} \tag{43}$$

from which the singular specific kinetic energy profile can be computed. For notational convenience, Eq. (43) is rewritten as

$$P(\tilde{E}(s), s) = \lambda_t^* \tag{44}$$

where

$$P(E,s) = 2\sqrt{2}mE^{3/2}\left.\frac{\partial D}{\partial E}\right|_{(E,s)} \tag{45}$$

for any $E > 0$.

Proposition IV.1: Let $E^*(s)$ be the optimal specific kinetic energy profile for Problem 1 with corresponding optimal costate value λ_t^*. Let the function $\tilde{E}\colon [s_0, s_f] \to \mathbb{R}_+$ be defined via the equation $P(\tilde{E}(s), s) = \lambda_t^*$ for all $s \in [s_0, s_f]$. Suppose that the following is true for all $E \in [v_{\min}^2/2, v_{\max}^2/2]$ and $s \in [s_0, s_f]$:

$$\frac{\partial^2 D(E,s)}{\partial E^2} + \frac{3}{2E}\frac{\partial D(E,s)}{\partial E} > 0 \tag{46}$$

Then, for all $s \in [s_0, s_f]$, $P(E^*(s), s) > \lambda_t^*$ if and only if $E^*(s) > \tilde{E}(s)$, and $P(E^*(s), s) < \lambda_t^*$ if and only if $E^*(s) < \tilde{E}(s)$.

Proof: Note that

$$\begin{aligned}\frac{\partial}{\partial E}\left(E^{3/2}\frac{\partial D(E,s)}{\partial E}\right) &= E^{3/2}\frac{\partial^2 D(E,s)}{\partial E^2} + \frac{3}{2}E^{1/2}\frac{\partial D(E,s)}{\partial E} \\ &= E^{3/2}\left(\frac{\partial^2 D(E,s)}{\partial E^2} + \frac{3}{2E}\frac{\partial D(E,s)}{\partial E}\right) > 0\end{aligned}$$

Therefore, $E^{3/2}\partial D(E,s)/\partial E$ increases monotonically with respect to E for any fixed $s \in [s_0, s_f]$. The following expression holds by the definition of P and λ_t^*:

$$P(E^*(s), s) - \lambda_t^* = 2\sqrt{2}m\left(E^{*3/2}(s)\left.\frac{\partial D}{\partial E}\right|_{(E^*(s),s)} - \tilde{E}^{3/2}(s)\frac{\partial \tilde{D}}{\partial E}\right)$$

and the claim of this proposition can be easily verified using the monotonicity of the function $E^{3/2}\partial D(E,s)/\partial E$ with respect to E.

With $E^*(s)$, λ_t^*, and $\tilde{E}(s)$ as in Proposition IV.1, the singular control $\tilde{T}$ can be obtained by

$$\tilde{T}(s) = m(\tilde{E}'(s) + D(\tilde{E}(s), s) + g\,\sin\gamma(s)) \tag{47}$$

It is clear that if $E^*(s)$ contains a singular arc on $[s_a, s_b] \subseteq [s_0, s_f]$, then the function $\tilde{E}(s)$ defined in Proposition IV.1 satisfies $\tilde{E}(s) = E^*(s)$ for all $s \in [s_a, s_b]$.

Suppose now that there exists $(s_a, s_b) \subseteq [s_0, s_f]$ such that $E^*(s) = \tilde{E}(s)$, but $\tilde{T}(s) > T_{\max}$ or $\tilde{T}(s) < T_{\min}$. It follows that the corresponding optimal thrust profile cannot contain any singular thrust subarc. Therefore, in the sequel it is assumed that $\tilde{T}(s) \in [T_{\min}, T_{\max}]$ for all $s \in (s_a, s_b)$. This assumption is valid as long as the aircraft is in a normal flight condition, and the path is smooth enough, in the sense that the path angle and the heading angle change slowly along the path.

According to the PMP when the state constraints (32) and (33) are not active the optimal control is composed of extremals corresponding to $T_{\max}$, $T_{\min}$, and $\tilde{T}$. The singular specific kinetic energy $\tilde{E}$ and the corresponding thrust profile $\tilde{T}$ are not readily known, because they depend on the unknown parameter λ_t^*, which further depends on the final time t_f. Furthermore, although there is a finite number of extremal controls, the possible combinations of the resulting extremals can be large. Hence, it is necessary to identify the switching structure for the different extremals along with the associated switching times in order to obtain the optimal solution.

B. Optimality of the Singular Arcs

An admissible singular control $\tilde{T}(s)$, in addition to the constraint $T_{\min} \le \tilde{T}(s) \le T_{\max}$, must satisfy the generalized Legendre–Clebsch condition [30]

$$\frac{\partial}{\partial T}\left[\frac{\mathrm{d}^2}{\mathrm{d}s^2}\left(\frac{\partial H}{\partial T}\right)\right] \le 0 \tag{48}$$

if it is to be part of the optimal trajectory. Differentiating the Hamiltonian with respect to s one obtains

$$\frac{\mathrm{d}^2}{\mathrm{d}s^2}\left(\frac{\partial H}{\partial T}\right) = \frac{\lambda_E'(s)}{m}\frac{\partial \tilde{D}}{\partial E} + \left(\frac{\lambda_E(s)}{m}\frac{\partial^2 \tilde{D}}{\partial E^2} - \frac{3}{4\sqrt{2}m}\tilde{E}^{-5/2}\lambda_t^*\right)\tilde{E}'(s)$$

Using Eq. (30) and the fact that $\lambda_E(s) = -m$ along the singular arc it follows that

$$\frac{\partial}{\partial T}\left[\frac{\mathrm{d}^2}{\mathrm{d}s^2}\left(\frac{\partial H}{\partial T}\right)\right] = -\frac{1}{m}\left(\frac{\partial^2 \tilde{D}}{\partial E^2} + \frac{3}{4\sqrt{2}m}\tilde{E}^{-5/2}\lambda_t^*\right) \tag{49}$$

Since $\tilde{E}(s)$ satisfies Eq. (44) it follows that

$$\lambda_t^* = 2\sqrt{2}m\tilde{E}^{3/2}\frac{\partial \tilde{D}}{\partial E} \tag{50}$$

By eliminating λ_t^* from Eq. (49) and by using Eq. (44), Eq. (49) can be written as

$$\frac{\partial}{\partial T}\left[\frac{\mathrm{d}^2}{\mathrm{d}s^2}\left(\frac{\partial H}{\partial T}\right)\right] = -\frac{\partial^2 \tilde{D}}{\partial E^2} - \frac{3}{2\tilde{E}}\frac{\partial \tilde{D}}{\partial E} \tag{51}$$

which is negative as long as Eq. (46) holds. Hence, along the singular arcs, the generalized Legendre–Clebsch condition is satisfied when Eq. (46) is valid, in which case these arcs can be part of the optimal trajectory.

Remark 1: Before applying the energy-optimal algorithm proposed later in this paper it is necessary to first verify condition (46), because this condition is essential for Proposition VI.1 and the optimality of the singular arc, which form the basis for the subsequent analysis. In particular, when the airspeed of the aircraft is low (typically, <0.6 Mach), the aerodynamic parameters C_{D_0} and K are approximately constant. In such a case, it can be verified analytically that Eq. (46) holds. When the Mach number of the aircraft is close to 1 the Mach number dependence of C_{D_0} and K usually cannot be neglected, and Eq. (46) can only be verified numerically, in general.

C. Optimal Switching Structure Involving Singular Arcs

When solving an optimal control problem with singular arcs, and because the optimal switching structure is not known in advance, it is a common practice to assume initially a certain fixed switching structure according to which the switching times are computed. This approach, although straightforward, may lead to a suboptimal solution. As shown in the subsequent analysis the switching structure of the optimal solution to Problem 1 can be uniquely determined owing to the special properties of this problem. The following theorem is key regarding the switching structure of the solution to Problem 1.

Theorem IV.1: Let $E^*(s)$ be the optimal specific kinetic energy profile for Problem 1, let the optimal costate valueλ_t^*, and let $\tilde{E}\colon [s_0, s_f] \to \mathbb{R}_+$ be the function defined by $P(\tilde{E}(s), s) = \lambda_t^*$. Consider a subinterval $(s_a, s_b) \subset [s_0, s_f]$ such that $\underline{g}_w(s) < E^*(s) < \bar{g}_w(s)$ for all $s \in (s_a, s_b)$. If $E^*(s) < \tilde{E}(s)$, (respectively, $E^*(s) > \tilde{E}(s)$) for all $s \in (s_a, s_b) \subset [s_0, s_f]$, then the corresponding optimal control $T^*(s)$ does not contain any switching from $T_{\min}$ to $T_{\max}$, (respectively, $T_{\max}$ to $T_{\min}$) on (s_a, s_b).

Proof: Assume that $E^*(s) < \tilde{E}(s)$ for all $s \in (s_a, s_b)$, and assume $T^*(s) = T_{\min}$ on (s_a, τ) and $T^*(s) = T_{\max}$ on (τ, s_b), where $\tau \in (s_a, s_b)$ is the switching point from $T_{\min}$ to $T_{\max}$. Because the state constraints are not saturated on (s_a, s_b) the optimal costate λ_E^* is continuous on (s_a, s_b). Because $T^*(s) = T_{\min}$ on (s_a, τ), and $T^*(s) = T_{\max}$ on (τ, s_b), it follows that $1 + \lambda_E^*(s)/m > 0$ on (s_a, τ), and $1 + \lambda_E^*(s)/m < 0$ on (τ, s_b) according to Eq. (42), and $\lambda_E^*(\tau) = -m$ by the continuity of λ_E^*.

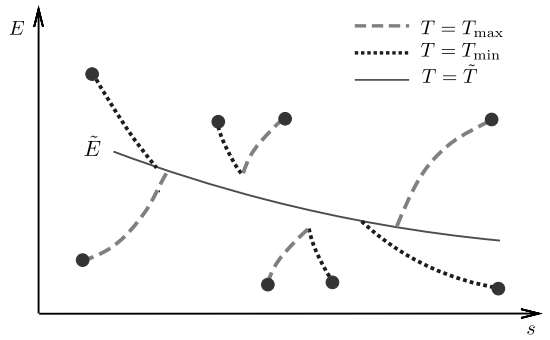

Fig. 1 Optimal switching structures.

According to Eq. (39) the derivative of the costate at τ is given by

$$\begin{aligned}\lambda_E^{*\prime}(\tau) &= \lambda_E^*(\tau)\frac{\partial D(E^*,\tau)}{\partial E} + \frac{1}{2\sqrt{2}}E^{*-3/2}(\tau)\lambda_t^* \\ &= -m\frac{\partial D(E^*,\tau)}{\partial E} + \frac{1}{2\sqrt{2}}E^{*-3/2}(\tau)\lambda_t^* \\ &= -\frac{1}{2\sqrt{2}}(E^*)^{-3/2}(\tau)(P(E^*(\tau),\tau) - \lambda_t^*)\end{aligned}$$

where Eqs. (44) and (45) are used for the derivation. Following Proposition IV.1, $\lambda_E^{*\prime}(\tau) > 0$ because the above expression is positive when $E^*(\tau) < \tilde{E}(\tau)$. Because $\partial D/\partial E$ is continuous with respect to s, $\lambda_E^{*\prime}(s)$ is also continuous with respect to s. Hence, $\lambda_E^{*\prime}(s) > 0$ is in a neighborhood of τ. However, this implies that given $1 + \lambda_E^*(s)/m > 0$ on (s_a, τ), there exists $\varepsilon > 0$ such that $1 + \lambda_E^*(s)/m > 0$ for all $s \in (\tau, \varepsilon) \subseteq (\tau, s_b)$, which is a contradiction to the fact that $1 + \lambda_E^*(s)/m < 0$ on (τ, s_b). Therefore, if $E^*(s) < \tilde{E}(s)$ on (s_a, s_b), the optimal thrust contains no switch from $T_{\min}$ to $T_{\max}$ on (s_a, s_b). The proof for the case $E^*(s) > \tilde{E}(s)$ is similar, and hence it is omitted.

Theorem IV.1 narrows down the possible switching combinations of the optimal control T^* for Problem 1. The valid switching structures above and below $\tilde{E}$ are illustrated in Fig. 1. In contrast, the switching structures in Fig. 2 are not optimal.

Given the optimal costate value λ_t^*, $\tilde{E}(s)$ can be computed from the expression $P(\tilde{E}(s), s) = \lambda_t^*$ for all $s \in [s_0, s_f]$. If the optimal specific kinetic energy E^* contains a singular arc on a subinterval then $E^* = \tilde{E}$ on this subinterval. The optimal specific kinetic energy E^* can be obtained by first identifying the segments of $\tilde{E}$ and then choosing the optimal structure and the corresponding switching times.

V. State Constraints and the Relaxed Problem

If the state constraints (32) and (33) in Problem 1 are not active along the optimal solution the optimal control input can be easily determined based on the results in Sec. IV. However, in general, the optimal solution to Problem 1 contains active state constraints. Specifically, when either the state constraint (32) or the constraint (33) is active along a certain part of the optimal specific kinetic energy solution E^* this part of E^* is called a *state constrained arc*. The corresponding control is referred to as a *state constrained control*. Hence, when the optimal solution contains state constrained arcs, it is necessary to identify the intervals on which state constraints (32) and (33) are active, which is usually not a straightforward task.

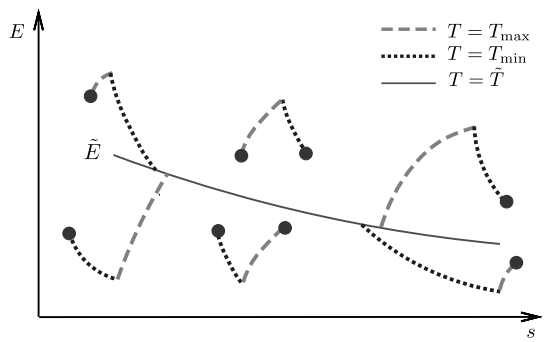

Fig. 2 Nonoptimal switching structures.

In this section, a relaxed version of Problem 1 is formulated by partially relaxing the state constraints (32) and (33) on certain intervals. The optimal solution to this relaxed problem can be determined in an semi-analytic way and will function as a key step in our proof regarding the optimal solution to the original Problem 1 in Sec. VI. B.

Before introducing the relaxed problem some additional notation needs to be presented as below. For any subset $\Gamma_U \subseteq [s_0, s_f]$ define

$$\bar{g}_{\Gamma_U}(s) = \begin{cases} \bar{g}_w(s), & s \in \Gamma_U, \\ M, & s \in [s_0, s_f] \setminus \Gamma_U \end{cases}$$

where $M > 0$ is a number large enough such that $E(s) < M$ is always satisfied on $[s_0, s_f]$ by any feasible specific kinetic energy profile $E(s)$. By choosing a subset Γ_U of interest and enforcing the state constraint $E(s) \le \bar{g}_{\Gamma_U}(s)$ for all $s \in [s_0, s_f]$ it can be ensured that the optimal solution E^* satisfies $E^*(s) \le g_w(s)$ on Γ_U while remaining unconstrained on $[s_0, s_f] \setminus \Gamma_U$. Similarly, also define

$$\underline{g}_{\Gamma_L}(s) = \begin{cases} \underline{g}_w(s), & s \in \Gamma_L, \\ 0, & s \in [s_0, s_f] \setminus \Gamma_L \end{cases}$$

By enforcing the constraint $E(s) \ge \underline{g}_{\Gamma_L}(s)$ instead of the constraint $E(s) \ge \underline{g}_w(s)$, the later constraint is relaxed on $[s_0, s_f] \setminus \Gamma_L$. Next, a modified version for Problem 1 is introduced by relaxing the original state constraints (32) and (33) on certain subintervals.

Problem 2 (Minimum-energy path-tracking problem with fixed TOA) Let $\Gamma_U, \Gamma_L \subseteq [s_0, s_f]$. Minimize the energy cost (29) subject to constraints (30), (31), (34), and (35)–(38), and the state bounds

$$E(s) - \bar{g}_{\Gamma_U}(s) \le 0 \tag{52}$$

$$\underline{g}_{\Gamma_L}(s) - E(s) \le 0 \tag{53}$$

for all $s \in [s_0, s_f]$.

Similarly, one can also form the relaxed minimum-time and the relaxed maximum-time path-tracking problems with state constraints (52) and (53) instead of (32) and (33). For the sake of brevity the formal definitions for these problems are not introduced here, because they are self-evident from the definition of Problem 2. Note that when $\Gamma_U = \Gamma_L = [s_0, s_f]$ then Problem 2 is identical to Problem 1, and the same is true for the minimum-time and maximum-time problems as well.

Because the unconstrained solution to an optimal control problem has the same or better optimality characteristics than a constrained one a constraint is, in general, not active unless it is violated by the optimal solution of the unconstrained problem.[‡] This property is stated formally by the next lemma.

Lemma V.1: Consider the following two optimal control problems:

Problem A	Problem B
$\min_u J(x,u)$	$\min_u J(x,u)$
s.t. $\dot{x}(t) = f(x(t),u(t))$,	s.t. $\dot{x}(t) = f(x(t),u(t))$,
$g_1(x(t),u(t)) \le 0$,	$g_1(x(t),u(t)) \le 0$,
$g_2(x(t),u(t)) \le 0$,	$t \in [t_0, t_f]$
$t \in [t_0, t_f]$,	$x(t_0) = x_0,\ x(t_f) = x_f$
$x(t_0) = x_0,\ x(t_f) = x_f$	

Let x_A^* be the optimal solution and u_A^* be the corresponding optimal control to Problem A and let x_B^* and u_B^* be the optimal solution and corresponding optimal control to Problem B. Then the following statements are true:

[‡]The only exception is the trivial case when along the unconstrained optimal solution certain constraints are active but not violated.

1) If $g_2(x_B^*(t), u_B^*(t)) \le 0$ for all $t \in [t_0, t_f]$ then $J(x_B^*, u_B^*) = J(x_A^*, u_A^*)$. Furthermore, if either Problem A or Problem B has a unique solution then $x_A^* = x_B^*$ and $u_A^* = u_B^*$.

2) If Problem B has a unique solution and $g_2(x_B^*(t), u_B^*(t)) > 0$ for some $t \in [t_0, t_f]$ then $J(x_A^*, u_A^*) > J(x_B^*, u_B^*)$.

Proof of Lemma V.1: Consider the first statement. Because (x_A^*, u_A^*) is the optimal solution to Problem A and (x_B^*, u_B^*) is a feasible solution to Problem A, it follows that $J(x_A^*, u_A^*) \le J(x_B^*, u_B^*)$ by the optimality of (x_A^*, u_A^*). On the other hand (x_A^*, u_A^*) satisfies all constraints in Problem B, so (x_A^*, u_A^*) is a feasible solution to Problem B. Consequently, $J(x_A^*, u_A^*) \ge J(x_B^*, u_B^*)$ by the optimality of (x_B^*, u_B^*) for Problem B. Therefore, $J(x_B^*, u_B^*) = J(x_A^*, u_A^*)$. It follows that $x_A^* = x_B^*$ and $u_A^* = u_B^*$, otherwise both Problem A and Problem B have nonunique solutions.

Now proceed to the second statement. As in the preceding proof, because (x_A^*, u_A^*) is a feasible solution to Problem B, it follows that $J(x_A^*, u_A^*) \ge J(x_B^*, u_B^*)$ by the optimality of (x_B^*, u_B^*) for Problem B. Because $g_2(x_B^*(t), u_B^*(t)) > 0$ for some $t \in [t_0, t_f]$, and $g_2(x_A^*(t), u_A^*(t)) \le 0$ for all $t \in [t_0, t_f]$, it follows that (x_B^*, u_B^*) and (x_A^*, u_A^*) are not identical. By the uniqueness of (x_B^*, u_B^*) it follows that $J(x_A^*, u_A^*) > J(x_B^*, u_B^*)$.

According to Lemma V.1 if the optimal solution to the relaxed Problem 2 does not violate the state constraints (32) and (33), then it is also the optimal solution to Problem 1. This argument is used in Sec. VI.B below to show the main result of this paper.

VI. Optimal Switching Structure Involving State-Constrained Arcs

A. Solution to the Relaxed Problem

The analysis in Sec. IV is valid when the state constraints (32) and (33) are inactive. This section considers the case when the state constraint (32) or (33) is active on part of the optimal trajectory. If the upper state constraint is saturated then $T^* = \bar{T}_w$, which is the thrust required to maintain $E^* = \bar{g}_w$. Similarly, if the lower state constraint is saturated then $T^* = \underline{T}_w$, which is the thrust required to maintain $E^* = \underline{g}_w$. Clearly, for feasibility, it is required that $\underline{T}_w$, $\bar{T}_w \in [T_{\min}, T_{\max}]$ on the corresponding domain for feasibility. For an arbitrary geometric path the optimal control T^* for the minimum-energy path-following problem is composed of bang–bang control $T_{\min}$ and $T_{\max}$, singular control $\tilde{T}$, and state constrained control $\bar{T}_w$ and $\underline{T}_w$ arcs.

The minimum-time path-following problem has been solved in [22]. This method can be modified to provide the maximum flight time along a given geometric path. The details are omitted for the sake of brevity. The maximum flight time scheme corresponds to the pointwise minimization of the specific kinetic energy along the path. This is the opposite of the minimum-time problem, which seeks to maximize pointwise the specific kinetic energy along the path. Note that, for any given path, an upper bound of the flight time exists, because the speed of a fixed-wing aircraft must be higher than a certain value to avoid stall.

Lemma VI.1: Let $E_U^*(s)$ be the minimum-time path-following specific kinetic energy profile with flight time $t_{\min}$, and let $E_L^*(s)$ be the maximum-time path-following specific kinetic energy profile with flight time $t_{\max}$ subject to the same boundary conditions and state constraints as in Eqs. (30)–(36). Let $E^*(s)$ be the optimal specific kinetic energy profile for the minimum-energy path-following problem with fixed flight time t_f. Then the following inequalities hold

$$t_{\min} \le t_f \le t_{\max} \tag{54}$$

$$E_L^*(s) \le E^*(s) \le E_U^*(s), \qquad s \in [s_0, s_f] \tag{55}$$

Proof: The inequalities in Eq. (54) involving $t_{\min}$ and $t_{\max}$ are obvious. To show the inequalities in Eq. (55), suppose, without loss of generality, that $E^*(s_a) > E_U^*(s_a)$ for some $s_a \in [s_0, s_f]$. Because both E^* and E_U^* are feasible specific kinetic energy profiles $\bar{E} = \max\{E^*, E_U^*\}$ is also a feasible specific kinetic energy profile, for example, $\bar{E}(s)$ satisfies the boundary conditions and state constraints and can be tracked with the available control inputs. Then $\bar{E} \ge E_U^*$ on $[s_0, s_f]$ and $\bar{E}(s) > E_U^*(s)$ on at least one interval containing s_a, following the continuity of E^*. Hence, for $\bar{E}$ the total flight time would be smaller than $t_{\min}$, which is a contradiction, because $t_{\min}$ is the minimum-time solution. The inequality $E_L^*(s) \le E^*(s)$ can be proved in a similar manner.

According to Lemma VI.1 the fixed-time energy-optimal specific kinetic energy E^* is bounded by the minimum-time solution E_U^* and the maximum-time solution E_L^*. Furthermore, based on Theorem IV.1, it can be shown that $E^*(s) = E_U^*(s)$ or $E^*(s) = E_L^*(s)$ on certain subintervals. This property of E^* is characterized by the following lemma.

Lemma VI.2: Let $E^*(s)$ be the optimal specific kinetic energy solution to Problem 1, and let $\tilde{E}$ be defined on $[s_0, s_f]$ by $P(\tilde{E}(s), s) = \lambda_t^*$, where λ_t^* is the corresponding optimal costate value. Let $E_U^*(s)$ and $E_L^*(s)$ be the optimal specific kinetic energy solutions to the minimum-time and maximum-time path-tracking problems, respectively. Furthermore, let

$$\Gamma_U = \{s | E_U^*(s) < \tilde{E}(s), s \in [s_0, s_f]\} \tag{56}$$

$$\Gamma_L = \{s | E_L^*(s) > \tilde{E}(s), s \in [s_0, s_f]\} \tag{57}$$

Suppose that $E^*(s) > \underline{g}_w(s)$ for all $s \in [s_0, s_f] \setminus \Gamma_L$, and $E^*(s) < \bar{g}_w(s)$ for all $s \in [s_0, s_f] \setminus \Gamma_U$, then $E^*(s) = E_U^*(s)$ for all $s \in \Gamma_U$, and $E^*(s) = E_L^*(s)$ for all $s \in \Gamma_L$.

Proof: See the Appendix.

Lemma VI.2, along with Lemma V.1, is used to characterize the state constrained arcs in the optimal specific kinetic energy profile $E^*(s)$. Specifically, given the state constraints, first compute the optimal solution of a certain relaxed problem to identify the state constrained arcs. Subsequently, the solution of the relaxed (nonconstrained) problem can be used to construct the solution of the original problem with state constraints.

In general, the minimum-time and maximum-time solutions of the relaxed problems are different from the corresponding solutions of the original (nonrelaxed) problem. However, as shown by the following proposition, by choosing carefully where the constraints are relaxed, the minimum-time and maximum-time solutions do not change on certain subintervals.

Proposition VI.1: Let $\tilde{E}$ be defined on $[s_0, s_f]$ by $P(\tilde{E}(s), s) = \lambda_t$ for a certain costate value λ_t such that $\tilde{T} \in [T_{\min}, T_{\max}]$, where $\tilde{T}$ is given by Eq. (47). Let Γ_U and Γ_L as in Eqs. (56) and (57), where $E_U^*(s)$ and $E_L^*(s)$ are the specific kinetic energy solutions to the minimum-time and maximum-time path-tracking problems, respectively, with constraints (32) and (33). Let $E_{U_r}^*(s)$ and $E_{L_r}^*(s)$ be the specific kinetic energy solutions to the relaxed minimum-time and maximum-time path-tracking problems, respectively, with constraints $E(s) \le \bar{g}_{\Gamma_U}(s)$ and $E(s) \ge \underline{g}_{\Gamma_L}(s)$ instead of Eqs. (32) and (33). Then $E_U^*(s) = E_{U_r}^*(s)$ for all $s \in \Gamma_U$, and $E_L^*(s) = E_{L_r}^*(s)$ for all $s \in \Gamma_L$.

Proof: See the Appendix.

B. Optimal Specific Kinetic Energy Solution

In this section, the main result of the paper is provided. Specifically, the optimal solution to Problem 1 is given by Theorem VI.1 below. As mentioned earlier, the proof of the theorem takes advantage of the optimal solution of the relaxed Problem 2 given in the preceding section. First, the optimal solution to the relaxed Problem 2 is characterized with the state constraints relaxed on some carefully selected subintervals. Then it is shown that this solution satisfies the state constraints in the original Problem 1, hence it is also the optimal solution to Problem 1. It is interesting to note that although the switching structure of the optimal solution to Problem 1 is complicated the expression of the optimal specific kinetic energy E^* can be written in a very succinct form in Eq. (58) as a combination of the minimum-time solution, the maximum-time solution, and energy-saving singular arcs. The precise proof is rather involved and, for the benefit of the interested reader, is given in the Appendix.

Theorem VI.1: Suppose there exists a real number λ_t, and a function $\tilde{E}$ given by $P(\tilde{E}(s), s) = \lambda_t$ for all $s \in [s_0, s_f]$ such that the specific kinetic energy E^* given by

$$E^*(s) = \begin{cases} E_L^*(s), & s \in \Gamma_L, \\ \tilde{E}(s), & s \in [s_0, s_f] \setminus (\Gamma_U \cup \Gamma_L), \\ E_U^*(s), & s \in \Gamma_U \end{cases} \tag{58}$$

satisfies the desired TOA, where $\Gamma_U = \{s | E_U^*(s) < \tilde{E}(s), s \in [s_0, s_f]\}$, and $\Gamma_L = \{s | E_L^*(s) > \tilde{E}(s), s \in [s_0, s_f]\}$. Then E^* is the optimal solution to Problem 1.

Proof: See the Appendix.

VII. Energy-Optimal Path-Tracking Algorithm

Theorem VI.1 characterizes the switching structure of the optimal solution to the aircraft energy-optimal path-tracking problem. Although E_U^* can be computed using the algorithm proposed in [22], and E_L^* can be computed in a similar manner, the optimal costate value λ_t^* is unknown. As a result, one is not readily able to choose the correct value of $\tilde{E}(s)$ for each $s \in [s_0, s_f]$ to construct the optimal specific kinetic energy according to Eq. (58). In this section a numerical algorithm is presented for solving Problem 1 by identifying the optimal costate value λ_t^*. This allows the computation of the associated function $\tilde{E}(s)$ from Eq. (44) and, subsequently, the optimal solution $E^*(s)$ from Eq. (58). To identify the constant λ_t^* and the associated singular arcs for a specific TOA it is necessary to search among a family of extremals associated with the prescribed geometric path for the correct value of λ_t^*.

The algorithm for identifying the minimum-energy path-tracking control is described in the Main Algorithm.

Remark 2: If the first derivative of the optimal specific kinetic energy E^* as given by the Main Algorithm does not exist at some point $s \in (s_0, s_f)$ then the value of the optimal thrust T^* is not well defined at s from Eq. (18). These are exactly the points where the derivative of E^* is discontinuous. The optimal thrust profile T^* is, therefore, discontinuous at those points. The limiting left/right values at these points of discontinuity of the thrust can be computed by the corresponding left/right limits of $E^{*\prime}$, which exist because E^* is a piecewise smooth function.

Step 4 of the Main Algorithm requires the computation of the optimal speed solution and the TOA for a specific extremal with costate value λ. This can be achieved using Algorithm 1.

According to the structure of the optimal specific energy profile in Eq. (58) it can be easily proved that the travel time τ_f of the energy-optimal solution decreases monotonically with increasing λ_t, because $\tilde{E}(s)$ increases monotonically with respect to λ_t for all $s \in [s_0, s_f]$ according to the definition of $\tilde{E}$ as in Eq. (44). In the Newton–Raphson algorithm with adjusted bounds used in step 4 of the Main Algorithm a bisection step is taken whenever the Newton–Raphson algorithm would take the solution outside the prescribed bounds. Because a bisection method is guaranteed to converge given the monotonicity property of the problem such a hybrid method is also guaranteed to converge, and the Newton–Raphson steps can speed up the convergence.

VIII. Numerical Examples

Next, the proposed energy-optimal tracking algorithm is validated using a three-dimensional landing trajectory, as shown in Fig. 3. The initial position of the aircraft is $(-135, -92, 6)$ km and the final position is $(0, 0, 0)$ km. The initial speed is $v_0 = 220$ m/s, and the final speed is $v_f = 95$ m/s. Both the initial and final path angles are 0 deg. The initial heading angle is 0 deg, and the final heading angle is -20 deg. The horizontal projection of the trajectory contains two turning maneuvers, as shown in Fig. 4.

The speed and control bounds considered during the time parameterization process are $M_a \leq 0.8$, where M_a is the Mach number, $C_{L_{\min}} = -0.47$, $C_{L_{\max}} = 1.73$, $\phi_{\min} = -15$ deg, $\phi_{\max} = 15$ deg, $T_{\min} = 0$. The wing surface area $S = 510.97$ m^2, the mass $m = 288,938$ kg. These data correspond approximately to a Boeing

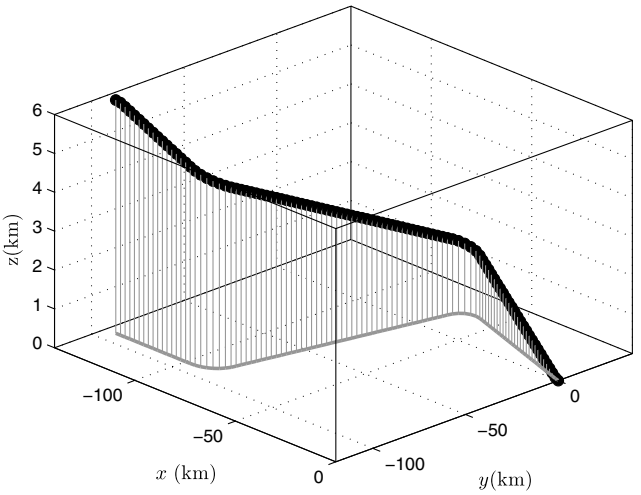

Fig. 3 Three-dimensional geometric trajectory.

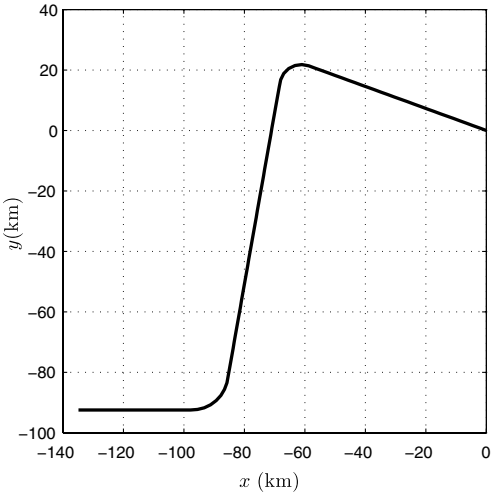

Fig. 4 *X-y* plane projection of the geometric trajectory.

747 aircraft. The aerodynamic parameters K and C_{D_0} are taken from [32] and stored in lookup tables. It has been verified numerically that Eq. (46) hold for any subsonic flight along the path. The dependence of the maximum thrust $T_{\max}(N)$ on the altitude z and Mach number M_a is taken into account by the following formula

$$T_{\max}(M_a, z) = (-0.007236z + 146.1968) \times (e^{-1.97967M_a + 8.23} + 2133)N$$

which fits approximately to the JT9D-7F engine maximum thrust data for a total of four engines.

The path is processed using the algorithm introduced in the preceding section with different TOA requirements. Figures 5 and 6 show the optimal speed profiles for the minimum-energy aircraft path tracking for several TOA values. It can be seen from these figures that with different TOA values t_f different parts of the minimum-time and/or the maximum-time speed profile can be involved in the minimum-energy solution together with the corresponding singular arcs. Figures 7 and 8 are the minimum-energy control histories for $t_f = 1300$ s and $t_f = 1600$ s, respectively. In these figures, the throttle is the ratio of the actual thrust to the maximum thrust $T_{\max}$. It is clear that all solutions satisfy the speed and control constraints along the path.

To evaluate the fuel economy of the energy-optimal solution a fuel-optimal control problem was solved using a numerical optimal control approach with the fuel consumption model (27) as the cost function. The constraints of the fuel-optimal control problem are

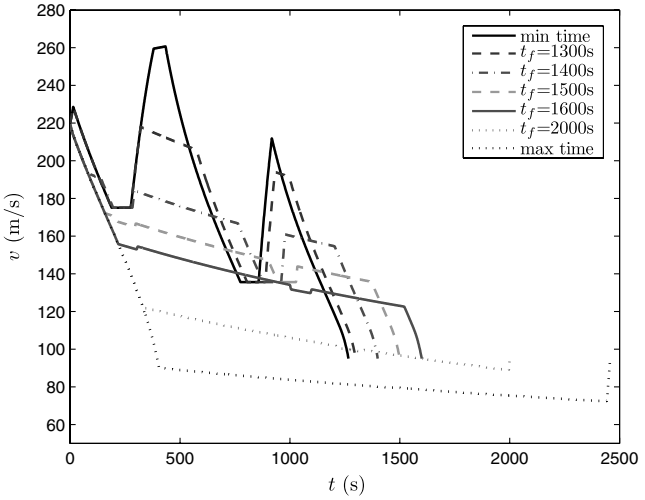

Fig. 5 Energy-optimal speed profiles with different TOA, path coordinate domain.

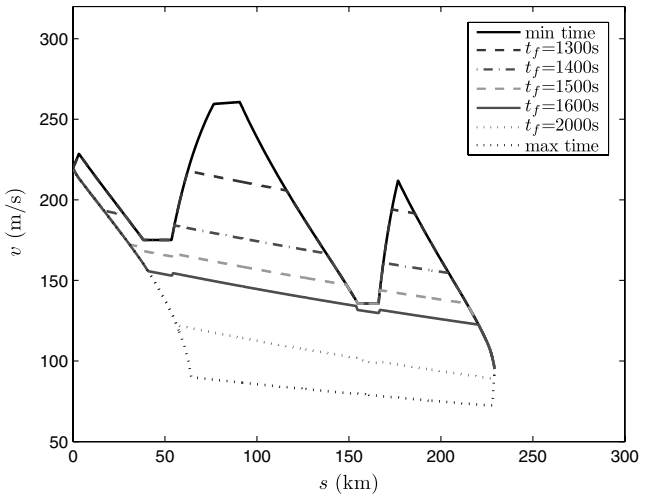

Fig. 6 Energy-optimal speed profiles with different TOA, time domain.

identical to those of Problem 1. The fuel-optimal control problem was converted into a nonlinear programming problem via direct transcription [11] and solved using the sparse nonlinear optimization software SNOPT [33]. The DENsity function-based Mesh Refinement Algorithm (DENMRA) in [34] was used to generate a mesh such that the state bounds (32) and (33) can be approximated more accurately with a limited number of grid points. The parameters for the computation of η_0 in Eq. (26) were stored in a lookup table and were provided to the nonlinear optimization solver.

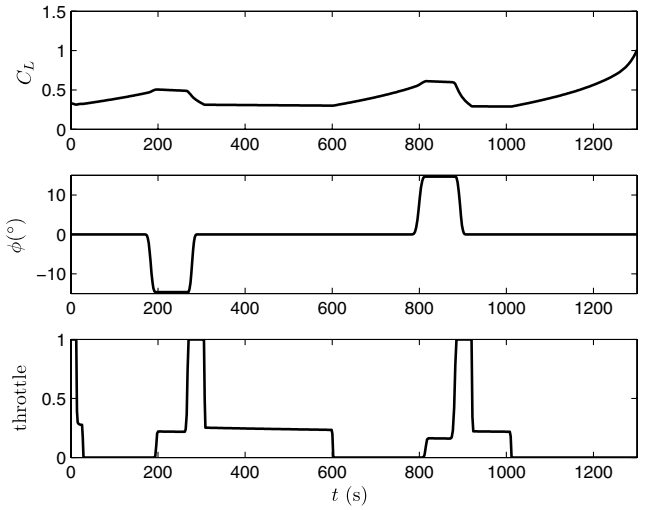

Fig. 7 Energy-optimal control histories with $t_f = 1300$ s.

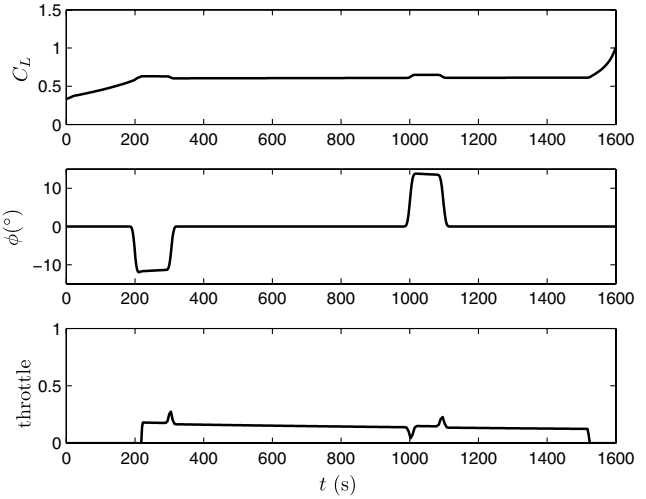

Fig. 8 Energy-optimal control histories with $t_f = 1600$ s.

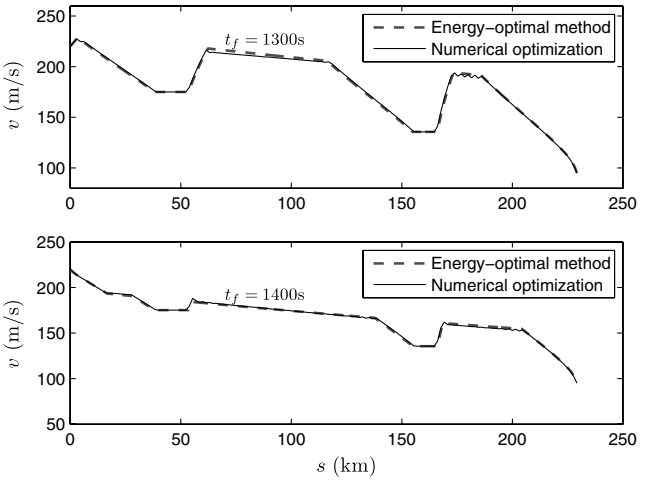

Fig. 9 Comparison of fuel-optimal and energy-optimal speed profiles, $t_f = 1300$ s and $t_f = 1400$ s.

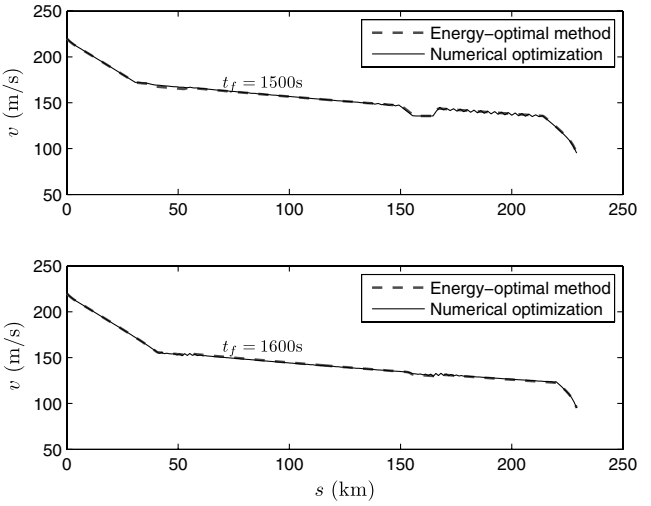

Fig. 10 Comparison of fuel-optimal and energy-optimal speed profiles, $t_f = 1500$ s and $t_f = 1600$ s.

Table 1 Fuel consumption comparison

	Fuel consumption, kg	
t_f (s)	Numerical optimization	Proposed method
1300	1809.2	1816.3
1400	1628.6	1632.9
1500	1612.0	1618.7
1600	1702.2	1704.8

The same four cases shown in Fig. 5 ($t_f = 1300$ s, 1400 s, 1500 s, 1600 s) were solved using the numerical optimal control approach for the minimum-fuel path-tracking problem, and the results were compared to those given by the energy-optimal path-tracking algorithm. The comparison of speed profiles are shown in Figs. 9 and 10. It is clear from these figures that the energy-optimal solutions are very close to the minimum-fuel solutions. Note that the singular arcs in the minimum-fuel problem cause numerical issues (oscillations along the singular arcs in Figs. 9 and 10). This is a well-known phenomenon when computing singular arcs using direct trajectory optimization methods.

To evaluate the effectiveness of the proposed energy-optimal operation method in terms of actual fuel-saving the fuel consumptions of the energy-optimal results are simulated using the same fuel consumption model (27) as used by the numerical approach. The fuel consumption simulation results are compared with the fuel-optimal numerical optimization results in Table 1. As shown in the table the simulated fuel consumption of the proposed method matches very well with the numerical optimization results.

The most appealing property of the proposed algorithm is its numerical efficiency. The computation time when using the standard numerical optimization approach is much longer than the one required by the proposed energy-optimal path-tracking algorithm: a MATLAB implementation of the energy-optimal path-tracking control algorithm finds the optimal solution in 3–6 s, while the nonlinear programming solver takes at least 5 min (and for some cases more than 20 min) to find a convergent fuel-optimal solution. The numerical efficiency of the algorithm allows the use of the proposed approach for computing good initial guesses for more accurate optimal trajectory generation solvers. In such a scenario, the semi-analytic solution provided by our approach can be further refined using more realistic, higher-fidelity aircraft models incorporating all effects (such as winds) neglected here, if needed. Previous results have shown a great increase in terms of numerical robustness and convergence of such trajectory generation solvers using this approach [21,24].

IX. Conclusions

The method presented in this paper computes the speed profile for an aircraft to follow a given three-dimensional geometric path with fixed time-of-arrival (TOA) while minimizing the energy along this path. It is shown that this problem accurately captures the fuel-optimal solution along a given path with fixed TOA. Such fuel-optimal solutions are useful for air traffic control (ATC) problems during the terminal (landing) phase. To generate the optimal solution the optimal switching structure of the problem is analyzed using the necessary conditions of optimality. The switching structure varies depending on the given TOA. However, for a given path and a fixed TOA, the structure is uniquely determined. It is proved that the energy-optimal solution is a combination of the minimum-time solution, the maximum-time solution, and energy-saving singular arcs. As verified by the numerical optimization results this method is computationally efficient and can be applied in real time for improving the fuel efficiency of airline scheduling and terminal ATC phase operations.

The major limitations of the proposed approach mainly hinge on simplifying modeling assumptions imposed on the problem to yield an analytically tractable solution. In particular, the effect of winds can have a significant impact on the solution and is not accounted for in the current formulation. A much more realistic model that accounts for both crosswinds and tail/headwinds can only be dealt with via purely numerical methods, using the no-wind solution as an initial guess. If, on the other hand, the effect of crosswinds can be neglected, the proposed approach can be adjusted to account for the effect of tail/headwinds whose main effect is the change of the estimated TOA. For instance, it can be shown that headwind or tailwind can be taken into consideration as long as lower and upper bounds $\bar{g}_w$ and $\underline{g}_w$ can be computed and that the condition (46) is satisfied. Although $\bar{g}_w$ can be easily obtained analytically $\underline{g}_w$ can only be computed numerically (alternatively, a conservative estimate of $\underline{g}_w$ is possible analytically). After these bounds have been computed the minimum-time and maximum-time solutions can be obtained, and, hence the energy-optimal solution can be constructed. A more comprehensive study of the wind effects, however, requires a separate thorough study and, thus, is left for future investigation.

Appendix: Proofs of Key Results

Proof of Lemma VI.2. First, it will be shown that $E^*(s) = E_U^*(s)$ for all $s \in \Gamma_U$. Let T_U^* and T^* be the thrust control associated with E_U^* and E^*, respectively. From Lemma VI.1 it follows that $E^*(s) \leq E_U^*(s)$ for all $s \in [s_0, s_f]$. Assume, ad absurdum, that there exists $\tau \in \Gamma_U$ such that $E^*(\tau) < E_U^*(\tau)$. Then, by the definition of Γ_U, $E^*(\tau) < \tilde{E}(\tau)$. Let $q = \inf\{s | E^*(s) = E_U^*(s), s \in [\tau, s_f]\}$, because $E^*(s_f) = E_U^*(s_f)$ q is well defined. Similarly, let $p = \sup\{s | E^*(s) = E_U^*(s), s \in [s_0, \tau]\}$, and because $E^*(s_0) = E_U^*(s_0)$ p is also well defined. Note that $E^*(s) < E_U^*(s)$ for all $s \in (p, q)$ by the fact $E^*(\tau) < E_U^*(\tau)$, the definitions of p, q, and the continuity of E^* and E_U^* (see Fig. A1). Because $E^*(s) < E_U^*(s) \leq \bar{g}_w(s)$ for all $s \in (p, q)$ the state constraint (32) is inactive along E^* for $s \in (p, q)$. Hence, $T^*(s)$ can only take the values of $T_{\max}$, $T_{\min}$, $\tilde{T}(s)$, or $\underline{T}_w(s)$ on (p, q). Because $\underline{E}^*(\tau) < \tilde{E}(\tau)$ it is true that $T^*(\tau) \neq \tilde{T}(\tau)$. Also, because $E^*(\tau) < \tilde{E}(\tau)$ it follows that $\tau \notin \Gamma_L$, and, therefore, $E^*(\tau) > \underline{g}_w(\tau)$, and it follows that either $T^*(\tau) = T_{\max}$ or $T^*(\tau) = T_{\min}$. Next, it will be shown that neither of these two options is possible.

First, consider the case $T^*(\tau) = T_{\min}$. It is claimed that $E^*(s) < \tilde{E}(s)$ for all $s \in (\tau, q)$. To see this, assume that $E^*(s) \geq \tilde{E}(s)$ for some $s \in (\tau, q)$. It then follows from the fact $E^*(\tau) < \tilde{E}(\tau)$ and the continuity of E^* and $\tilde{E}$ that the equation $E^*(\gamma) = \tilde{E}(\gamma)$ has at least one solution on (τ, q) (see Fig. A1). Let $\gamma = \inf\{s | E^*(s) = \tilde{E}(s), s \in (\tau, q)\}$. It follows that $E^*(\gamma) = \tilde{E}(\gamma)$ and $E^*(s) < \tilde{E}(s)$ for all $s \in (\tau, \gamma)$. Therefore, $(\tau, \gamma) \subseteq [s_0, s_f] \setminus \Gamma_L$, and it is true that $E^*(s) > \underline{g}_w(s)$ for all $s \in (\tau, \gamma)$. It follows that on (τ, γ) $T^*(s)$ can only take the values of $T_{\min}$ and $T_{\max}$. Because $E^*(s) < \tilde{E}(s)$ for all $s \in (\tau, \gamma)$ $T^*(s)$ cannot switch from $T_{\min}$ to $T_{\max}$ according to Theorem IV.1, and $T^*(s) = T_{\min}$ for all $s \in [\tau, \gamma)$. The trajectories $E^*(s)$ and $E^*(s)$ on (τ, γ) can be computed starting from $E^*(\gamma) = \tilde{E}(\gamma)$ at $s = \gamma$ by integrating backward Eq. (30) with $T^*(s) = T_{\min}$ and $\tilde{T}$, respectively. Because $T_{\min} \leq \tilde{T}(s)$, a straightforward application of the Comparison Lemma yields that $E^*(\tau) \geq \tilde{E}(\tau)$, leading to a contradiction. Hence, $E^*(s) < \tilde{E}(s)$ for all $s \in (\tau, q)$, and, thus, $T_{\min} \leq \tilde{T}(s)$ for all $s \in (\tau, q)$ according to Theorem IV.1. The last statement implies, however, that one can compute $E^*(\tau)$ and $E_U^*(\tau)$ on the interval (τ, q) starting at $s = q$ with initial conditions $E^*(q) = E_U^*(q)$ and integrating backward Eq. (30)

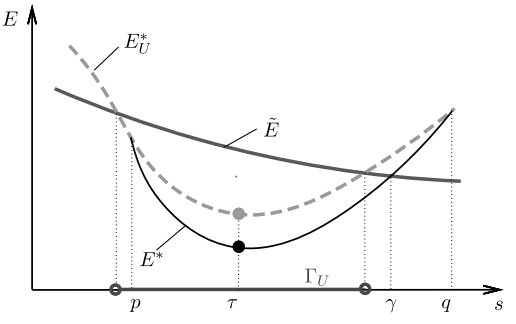

Fig. A1 Illustration for the Proof of Lemma VI.2.

Main Algorithm Main steps for energy-optimal flight path racking.

Compute the optimal solution for aircraft minimum-energy path-tracking operation with fixed TOA.
1) Compute the state bounds $\bar{g}_w(s)$, $\underline{g}_w(s)$ and the functions $c_1(s)$, $c_2(s)$, $c_3(s)$ in Problem 1 as in [22].
2) Compute and store the values of $P(E(s), s)$ from Eq. (44) on a selected, adequately fine, mesh $\mathcal{M}$ over the domain $[s_0, s_f] \times [E_{\min}, E_{\max}]$, where $[E_{\min}, E_{\max}]$ covers the possible range of the specific kinetic energy.
3) Compute the minimum-time solution $E_U^*(s)$ and the maximum-time solution $E_L^*(s)$ using the algorithm in [22]. Let the corresponding minimum and maximum TOA be $t_{\min}$ and $t_{\max}$, respectively. Proceed to the next step if $t_{\min} < t_f < t_{\max}$. Otherwise, quit the algorithm because the desired TOA is not possible, and the given problem does not have a solution.
4) Apply a Newton–Raphson algorithm with adjusted bounds of the solution [31] to find the optimal costate value λ_t^* such that $\tau_f = t_f$, where τ_f is given by Algorithm 1 below with $\lambda = \lambda_t^*$. Then the corresponding specific kinetic energy $E^*(s)$ associated with the costate value λ_t^*, which is returned by Algorithm 1, is the optimal solution with TOA equal to t_f.
5) Compute the optimal thrust $T^*(s)$, bank angle $\phi^*(s)$, and lift coefficient $C_L^*(s)$ histories using Eqs. (18), (23), and (24), respectively.

Algorithm 1 Optimal specific energy for given time costate value.

Compute the TOA τ_f and the corresponding optimal specific kinetic energy profile $E^*(s)$ for a given λ value.
1) Solve $P(\tilde{E}_\lambda(s), s) = \lambda$ for the function $\tilde{E}_\lambda(s)$ by interpolating the precomputed and stored data of $P(E(s), s)$ for the given path on the mesh $\mathcal{M}$.
2) Compute the optimal specific kinetic energy $E^*(s)$ for the given λ using formula (58) along with the computed maximum-time specific kinetic energy $E_L^*(s)$ and minimum-time specific kinetic energy $E_U^*(s)$.
3) Compute the TOA τ_f for $E^*(s)$ using $\tau_f = \int_{s_0}^{s_f} \frac{1}{\sqrt{2E^*(s)}}\,\mathrm{d}s$.
4) Return τ_f and $E^*(s)$.

using $T^*(s) = T_{\min}$ and $T_U^*(s)$, respectively, for all $s \in (\tau, q)$. Because $T_U^*(s) \geq T_{\min} = T^*(s)$ an application of the Comparison Lemma as before yields that $E^*(\tau) \geq E_U^*(\tau)$, which contradicts the assumption $E^*(\tau) < E_U^*(\tau)$.

Similarly, if $T^*(\tau) = T_{\max}$, one can prove in a similar manner that $E^*(\tau) < E_U^*(\tau)$ is also impossible. Hence, there does not exist $\tau \in \Gamma_U$ such that $E^*(\tau) < E_U^*(\tau)$, and, thus, it must be true that $E^*(s) = E_U^*(s)$ on Γ_U.

The proof for the other statement, $E^*(s) = E_L^*(s)$ for all $s \in \Gamma_L$, is similar, hence, is omitted.

Proof of Proposition VI.1. Noting that $E_U^*(s)$ is a feasible solution to the relaxed minimum-time problem one has $E_U^*(s) \leq E_{U_r}^*(s)$ for all $s \in [s_0, s_f]$ by the time optimality of $E_{U_r}^*$. Similarly, $E_L^*(s) \geq E_{L_r}^*(s)$ for all $s \in [s_0, s_f]$. Define

$$E(s) = \begin{cases} \min\{\max\{E_{U_r}^*(s), E_U^*(s)\}, \tilde{E}(s)\}, & s \in \Gamma_U, \\ E_U^*(s), & s \in [s_0, s_f] \setminus \Gamma_U \end{cases} \tag{A1}$$

By the definition of $E(s)$ and Γ_U, $E(s) \geq E_U^*(s)$ on $[s_0, s_f]$, and $E(s)$ is continuous. Furthermore, $E(s_0) = E_U^*(s_0) = E_0$, $E(s_f) = E_U^*(s_f) = E_f$, and $\underline{g}_w(s) \leq E(s) \leq \bar{g}_w(s)$ for all $s \in [s_0, s_f]$. Hence, $E(s)$ is a feasible solution to the minimum-time path-tracking problem with constraints (32) and (33).

If there exist $\tau \in \Gamma_U$ such that $E_{U_r}^*(\tau) > E_U^*(\tau)$ then by the definition of $E(s)$, $E(\tau) > E_U^*(\tau)$, and it follows from the continuity of E and E_U^* that $E(s) > E_U^*(s)$ in a neighborhood of τ. Hence,

$$\int_{s_0}^{s_f} \frac{1}{\sqrt{2E(s)}}\,\mathrm{d}s < \int_{s_0}^{s_f} \frac{1}{\sqrt{2E_U^*(s)}}\,\mathrm{d}s$$

which means that $E(s)$ has a shorter final time than $E_U^*(s)$, which is a contradiction because E_U^* is the minimum-time solution. Therefore, $E_U^*(s) = E_{U_r}^*(s)$ for all $s \in \Gamma_U$. Similarly, one can prove that $E_L^*(s) = E_{L_r}^*(s)$ for all $s \in \Gamma_L$. The proof is omitted for the sake of brevity.

Proof of Theorem VI.1. It can be easily verified that E^*, as defined by Eq. (58), satisfies the initial and final conditions, namely, $E^*(s_0) = E_0$ and $E^*(s_f) = E_f$. Consider now the relaxed energy-optimal Problem 2 with state constraints $E(s) \leq \bar{g}_{\Gamma_U}(s)$ and $E(s) \geq \underline{g}_{\Gamma_L}(s)$, for example, the state constraints (32) and (33) of the original energy-optimal problem are relaxed on $[s_0, s_f] \setminus \Gamma_U$ and $[s_0, s_f] \setminus \Gamma_L$, respectively. Let the optimal specific kinetic energy solution for this relaxed energy-optimal problem be E_r^*, let $\lambda_{t_r}^*$ be the associated optimal costate value, and let $\tilde{E}_r$ be defined on $[s_0, s_f]$ by $P(\tilde{E}_r(s), s) = \lambda_{t_r}^*$. Finally, let $T_r^*(s)$ denote the optimal control associated with $E_r^*(s)$, and let $T^*(s)$ denote the control associated with $E^*(s)$. By the definition of E^* $T_{\min} \leq T^*(s) \leq T_{\max}$ for all $s \in [s_0, s_f]$.

In the following, it will be shown that $E_r^*(s) = E^*(s)$ for all $s \in [s_0, s_f]$. Note that, because E_r^* and E^* have the same final time, this is equivalent to the nonexistence of a point $\tau \in (s_0, s_f)$ such that $E^*(\tau) < E_r^*(\tau)$ or of a point $\gamma \in (s_0, s_f)$ such that $E^*(\gamma) > E_r^*(\gamma)$. The proof will be given in terms of contradiction. There are three cases to consider. In each case, it will be shown that either $E^*(\tau) < E_r^*(\tau)$ is not possible for all $\tau \in (s_0, s_f)$ or $E^*(\gamma) > E_r^*(\gamma)$ is not possible for all $\gamma \in (s_0, s_f)$ (or both).

First, consider the case when $\lambda_{t_r}^* < \lambda_t$. It will be shown that, in this case, $E^*(\tau) < E_r^*(\tau)$ is not possible for all $\tau \in [s_0, s_f]$. By the definition of P in Eq. (44), $\tilde{E}_r(s) < \tilde{E}(s)$ for all $s \in [s_0, s_f]$. Let $E_{U_r}^*$ and $E_{L_r}^*$ be the minimum-time and maximum-time solutions to the relaxed problems with relaxed state constraints $E(s) \leq \bar{g}_{\Gamma_U}(s)$ and $E(s) \geq \underline{g}_{\Gamma_L}(s)$. Following Proposition VI.1, it is true that $E_{U_r}^*(s) = E_U^*(s)$ for $s \in \Gamma_U$, and $E_{L_r}^*(s) = E_L^*(s)$ for $s \in \Gamma_L$. Define $\Gamma_{L_r} = \{s | E_{L_r}^*(s) > \tilde{E}_r(s), s \in [s_0, s_f]\}$. Then from the fact that $E_{L_r}^*(s) = E_L^*(s) > \tilde{E}(s) > \tilde{E}_r(s)$ on Γ_L, it follows that $\Gamma_L \subseteq \Gamma_{L_r}$. Following Lemma VI.2, it is true that $E_r^*(s) = E_{L_r}^*(s)$ for all $s \in \Gamma_{L_r}$. Hence, $E_r^*(s) = E_{L_r}^*(s) = E_L^*(s) = E^*(s)$ for all $s \in \Gamma_L$. Similarly, for $s \in \Gamma_U$, it can be shown that $E_r^*(s) \leq E_{U_r}^*(s) = E_U^*(s) = E^*(s)$.

Thus, it has been shown that $E_r^*(s) \leq E^*(s)$ for all $s \in \mathcal{K}$, where $\mathcal{K} = \Gamma_U \cup \Gamma_L$, and, hence if there exists $\tau \in [s_0, s_f]$ such that $E_r^*(\tau) > E^*(\tau)$, necessarily it must be an element of the complement of $\mathcal{K}$ in $[s_0, s_f]$, namely, $\tau \in [s_0, s_f] \setminus \mathcal{K}$. But this leads to a contradiction. To see this, let $p = \sup\{s | E^*(s) = E_r^*(s), s \in [s_0, \tau]\}$. Note that p is well defined, because $E^*(s_0) = E_r^*(s_0) = E_0$. Similarly, let $q = \inf\{s | E^*(s) = E_r^*(s), s \in [\tau, s_f]\}$, also well defined, because $E^*(s_f) = E_r^*(s_f) = E_f$. Then $E_r^*(s) > E^*(s)$ for all $s \in (p, q)$, $E^*(p) = E_r^*(p)$ and $E^*(q) = E_r^*(q)$ by the continuity of E^* and E_r^*. Furthermore, it can be easily shown that $(p, q) \subseteq [s_0, s_f] \setminus \mathcal{K}$. Hence, $E_r^*(s) > E^*(s) = \tilde{E}(s) > \tilde{E}_r(s)$ for all $s \in (p, q)$. On the other hand, because the state constraints are relaxed on $[s_0, s_f] \setminus \mathcal{K}$ in the relaxed energy-optimal problem and $(p, q) \subseteq [s_0, s_f] \setminus \mathcal{K}$, E_r^* does not contain any active state constrained arc on (p, q). Therefore, either $T_r^*(s) = T_{\max}$ or $T_r^*(s) = T_{\min}$ for $s \in (p, q)$. In particular, either $T_r^*(\tau) = T_{\min}$ or $T_r^*(\tau) = T_{\max}$. If $T_r^*(\tau) = T_{\min}$, it must be true that $T_r^*(\tau) = T_{\min}$ for all $s \in (p, \tau)$,

because by Theorem IV.1 $T_r^*(s)$ cannot switch from $T_{\max}$ to $T_{\min}$ with $E_r^*(s) > \tilde{E}_r(s)$. Integrating forward (30) with initial conditions $E_r^*(p) = E^*(p)$ and noting that $T_r^*(s) = T_{\min} \leq T^*(s)$ a direct application of the Comparison Lemma as in the Proof of Lemma VI.2 leads to $E_r^*(\tau) \leq E^*(\tau)$, which is a contradiction. Similarly, it can be shown that $T_r^*(\tau) = T_{\max}$ also leads to the same contradiction by integrating backward on (τ, q). Hence, $E_r^*(\tau) > E^*(\tau)$ is not possible when $\lambda_{t_r}^* < \lambda_t$, which necessarily implies that $E_r^*(s) = E^*(s)$ for all $s \in [s_0, s_f]$ if $\lambda_{t_r}^* < \lambda_t$.

Consider now the case $\lambda_{t_r}^* > \lambda_t$. Using similar arguments as before, it can be shown that there does not exist $\gamma \in (s_0, s_f)$ such that $E^*(\gamma) > E_r^*(\gamma)$, for example, $E_r^*(s) = E^*(s)$ for all $s \in [s_0, s_f]$ if $\lambda_{t_r}^* > \lambda_t$.

For the case when $\lambda_{t_r}^* = \lambda_t$, $\tilde{E}_r(s) = \tilde{E}(s)$ for all $\in [s_0, s_f]$. It follows from Lemma VI.2 that $E_r^*(s) = E^*(s) = E_U^*(s) = E_{U_r}^*(s)$ on Γ_U and $E_r^*(s) = E^*(s) = E_L^*(s) = E_{L_r}^*(s)$ on Γ_L, yielding $\tau, \gamma \in [s_0, s_f] \setminus \mathcal{K}$. The application of the same argument as in the proof for the case $\lambda_{t_r}^* < \lambda_t$ (or the case $\lambda_{t_r}^* > \lambda_t$) also leads to a contradiction.

Hence, it has been shown that $E^*(s) = E_r^*(s)$ for all $s \in [s_0, s_f]$, in other words, E^* is the optimal solution to the relaxed Problem 2 with state constraints $E(s) \leq \bar{g}_{\Gamma_U}(s)$, and $E(s) \geq \underline{g}_{\Gamma_L}(s)$. Because $E^*(s) = E_U^*(s) \leq \bar{g}_w(s)$ for $s \in \Gamma_U$, $E^*(s) = E_L^*(s) \geq \underline{g}_w(s)$ for $s \in \Gamma_L$, and $\underline{g}_w(s) \leq E_L^*(s) < E^*(s) = \tilde{E}(s) < E_U^*(s) \leq \bar{g}_w(s)$ for $s \in [s_0, s_f] \setminus \mathcal{K}$ it is clear that $\underline{g}_w(s) \leq E^*(s) \leq \bar{g}_w(s)$ for all $s \in [s_0, s_f]$. Hence, $E^*(s)$ is a feasible solution to Problem 1. Because E^* is the optimal solution to the relaxed Problem 2, and it is a feasible solution for Problem 1, E^* is also the optimal solution to Problem 1 by Lemma V.1, and the proof is complete.

Acknowledgment

This work has been supported by NASA Ames Research Center, contract no. NNX08AB94A.

References

[1] Shin, K. G., and McKay, N. D., "Minimum-Time Control of Robotic Manipulators with Geometric Path Constraints," *IEEE Transactions on Automatic Control*, Vol. AC-30, No. 6, June 1985, pp. 531–541. doi:10.1109/TAC.1985.1104009

[2] Pfeiffer, F., and Johanni, R., "A Concept for Manipulator Trajectory Planning," *IEEE Journal of Robotics and Automation*, Vol. RA-3, No. 2, April 1987, pp. 115–123. doi:10.1109/JRA.1987.1087090

[3] Shiller, Z., and Lu, H.-H., "Computation of Path Constrained Time Optimal Motions with Dynamic Singularities," *Journal of Dynamic Systems, Measurement, and Control*, Vol. 114, No. 1, 1992, pp. 34–40. doi:10.1115/1.2896505

[4] Verscheure, D., Demeulenaere, B., Swevers, J., Schutter, J. D., and Diehl, M., "Time-Optimal Path Tracking for Robots: A Convex Optimization Approach," *IEEE Transactions on Automatic Control*, Vol. 54, No. 10, 2009, pp. 2318–2327. doi:10.1109/TAC.2009.2028959

[5] Asnis, I. A., Dmitruk, A. V., and Osmolovskii, N. P., "Solution of the Problem of the Energetically Optimal Control of the Motion of a Train by the Maximum Principle," *Computational Mathematics and Mathematical Physics*, Vol. 25, No. 6, 1985, pp. 37–44.

[6] Khmelnitsky, E., "On an Optimal Control Problem of Train Operation," *IEEE Transactions on Automatic Control*, Vol. 45, No. 7, July 2000, pp. 1257–1265. doi:10.1109/9.867018

[7] Holett, P. G., Pudney, P. J., and Vu, X., "Local Energy Minimization in Optimal Train Control," *Automatica*, Vol. 45, No. 11, 2009, pp. 2692–2698. doi:10.1016/j.automatica.2009.07.028

[8] Velenis, E., and Tsiotras, P., "Minimum-Time Travel for a Vehicle with Acceleration Limits: Theoretical Analysis and Receding Horizon Implementation," *Journal of Optimization Theory and Applications*, Vol. 138, No. 2, 2008, pp. 275–296. doi:10.1007/s10957-008-9381-7

[9] Kelley, H. J., "Flight Path Optimization with Multiple Time Scales," *Journal of Aircraft*, Vol. 8, No. 4, 1971, pp. 238–240. doi:10.2514/3.44261

[10] Lu, P., and Pierson, B. L., "Optimal Aircraft Terrain-Following Analysis and Trajectory Generation," *Journal of Guidance, Control, and Dynamics*, Vol. 18, No. 3, 1995, pp. 555–560. doi:10.2514/3.21422

[11] Betts, J. T., *Practical Methods for Optimal Control Using Nonlinear Programming*, Society for Industrial and Applied Mathematics, Philadelphia, PA, 2001, pp. 61–176.

[12] Bulirsch, R., Montrone, F., and Pesch, H. J., "Abort Landing in the Presence of Windshear as a Minimax Optimal Control Problem, Part I: Necessary Conditions," *Journal of Optimization Theory and Applications*, Vol. 70, No. 1, 1991, pp. 1–23. doi:10.1007/BF00940502

[13] Bulirsch, R., Montrone, F., and Pesch, H. J., "Abort Landing in the Presence of Windshear as a Minimax Optimal Control Problem, Part II: Multiple Shooting and Homotopy," *Journal of Optimization Theory and Applications*, Vol. 70, No. 2, 1991, pp. 223–254. doi:10.1007/BF00940625

[14] Steinbach, M. C., Bock, H. G., and Longman, R. W., "Time-Optimal Extension and Retraction of Robots: Numerical Analysis of the Switching Structure," *Journal of Optimization Theory and Applications*, Vol. 84, No. 3, 1995, pp. 589–616. doi:10.1007/BF02191987

[15] Cao, B., Dodds, G. I., and Irwin, G. W., "Constrained Time-Efficient and Smooth Cubic Spline Trajectory Generation for Industrial Robots," *IEEE Proceedings of Control Theory and Applications*, Vol. 144, No. 5, 1997, pp. 467–475. doi:10.1049/ip-cta:19971494

[16] Choset, H., Lynch, K., Hutchinson, S., Kantor, G., Burgard, W., Kavraki, L., and Thrun, S., *Principles of Robot Motion-Theory, Algorithms, and Implementation*, MIT Press, Cambridge, MA, June 2005, pp. 401–472.

[17] Karelahti, J., Virtanen, K., and Öström, J., "Automated Generation of Realistic Near-Optimal Aircraft Trajectories," *Journal of Guidance, Control, and Dynamics*, Vol. 31, No. 3, 2008, pp. 674–688. doi:10.2514/1.31159

[18] Frazzoli, E., *Robust Hybrid Control for Autonomous Vehicle Motion Planning*, Ph.D Thesis, Massachusetts Inst. of Technology, Cambridge, MA, 2001.

[19] Plaku, E., Kavraki, L. E., and Vardi, M. Y., "Motion Planning With Dynamics by a Synergistic Combination of Layers of Planning," *IEEE Transactions on Robotics*, Vol. 26, No. 3, 2010, pp. 469–482. doi:10.1109/TRO.2010.2047820

[20] Zhao, Y., and Tsiotras, P., "A Quadratic Programming Approach to Path Smoothing," *Proceedings of the American Control Conference*, San Francisco, CA, American Automatic Control Council, Evanston, IL, 2011, pp. 5324–5329.

[21] Bakolas, E., Zhao, Y., and Tsiotras, P., "Initial Guess Generation for Aircraft Landing Trajectory Optimization," *AIAA Guidance, Navigation, and Control Conference*, Portland, OR, AIAA Paper 2011-6689, 8–11 Aug. 2011.

[22] Zhao, Y., and Tsiotras, P., "Time-Optimal Parameterization of Geometric Path for Fixed-Wing Aircraft," AIAA Paper 2010-3352, 2010.

[23] Vossen, G., Rehbock, V., and Siburian, A., "Numerical Solution Methods for Singular Control with Multiple State Dependent Forms," *Optimization Methods and Software*, Vol. 22, No. 4, 2007, pp. 551–559. doi:10.1080/10556780600802924

[24] Zhao, Y., and Tsiotras, P., "Time-Optimal Path Following for Fixed-Wing Aircraft," *Journal of Guidance, Control, and Dynamics*, Vol. 36, No. 1, 2013, pp. 83–95. doi:10.2514/1.57471

[25] Miele, A., *Flight Mechanics, Vol. I: Theory of Flight Paths*, Addison Wesley Longman, Reading, MA, 1962, pp. 48–50.

[26] Mattingly, J. D., Heiser, W. H., and Pratt, D. T., *Aircraft Engine Design*, AIAA, New York, NY, 1987, pp. 55–71.

[27] Burrows, J. W., "Fuel-Optimal Aircraft Trajectories with Fixed Arrival Times," *Journal of Guidance, Control, and Dynamics*, Vol. 6, No. 1, 1983, pp. 14–19. doi:10.2514/3.19796

[28] Franco, A., Rivas, D., and Valenzuela, A., "Minimum-Fuel Cruise at Constant Altitude with Fixed Arrival Time," *Journal of Guidance, Control, and Dynamics*, Vol. 33, No. 1, 2010, pp. 280–285. doi:10.2514/1.46465

[29] Kelley, H. J., Kopp, R. E., and Moyer, H. G., *Singular Extremals, Topics in Optimization*, Academic Press, New York, NY, 1967.

[30] Bryson, A. E., and Ho, Y., *Applied Optimal Control-Optimization, Estimation and Control*, Hemispere, Washington, D.C., 1975, p. 135.

[31] Press, W. H., Teukolsky, S. A., Vetterling, W. T., and Flannery, B. P., *Numerical Recipes: The Art of Scientific Computing*, 3rd ed., Cambridge Univ. Press, New York, NY, Aug. 2007, p. 460.

[32] Mair, W. A., and Birdsall, D. L., *Aircraft Performance*, *Cambridge Aerospace Series*, Cambridge Univ. Press, Cambridge, U.K., 1996, p. 255.

[33] Gill, P. E., Murray, W., and Saunders, M. A., "SNOPT: An SQP Algorithm for Large-Scale Constrained Optimization," Univ. of California, Numerical Analysis Rept. 97-2, San Diego, La Jolla, CA, 1997, pp. 1–37.

[34] Zhao, Y., and Tsiotras, P., "Density Functions for Mesh Refinement in Numerical Optimal Control," *Journal of Guidance, Control, and Dynamics*, Vol. 34, No. 1, 2011, pp. 271–277. doi:10.2514/1.45852